*2017 International Nuclear Atlantic Conference - INAC 2017*
*Belo Horizonte, MG, Brazil, October 22-27, 2017*
*ASSOCIAÇÃO BRASILEIRA DE ENERGIA NUCLEAR – ABEN*

Agência Brasileira do ISBN
ISBN 978-85-99141-07-6
9 788599 141076

# STUDY OF TENSILE TEST BEHAVIOR OF AUSTENITIC STAINLESS STEEL TYPE 347 SEAMLESS THIN-WALLED TUBES IN COLD-WORKED CONDITION

**Clarice Terui[1] and Nelson B. de Lima[2]**
[1] Centro Tecnológico da Marinha em São Paulo - CTMSP
Centro Industrial Nuclear da Marinha - CINA
Rodovia Sorocaba-Iperó, km 12,5
18560-000 Iperó, SP
clarice.terui@marinha.mil.br

[2] Instituto de Pesquisas Energéticas e Nucleares (IPEN / CNEN - SP)
Av. Professor Lineu Prestes 2242
05508-000 São Paulo, SP
nblima@ipen.br

## ABSTRACT

These austenitic stainless steel type 347 seamless thin-walled tubes are potential candidates to be used in fuel elements of nuclear power plants (as PWR – Pressurized Water Reactor). So, their metallurgical condition and mechanical properties, as the tensile strength and yield strength, normally are very restrict in demanding project and design requirements. Several full size tensile tests at room temperature and high temperature (315ºC) were performed in these seamless tubes in cold-worked condition. The results of specified tensile and yield strengths were achieved but the elongation of the tube, in the geometry of the component, could not be measured at high temperature due to unconventional mode of rupture (helical mode without separation of parts). The average value of elongation was obtained from stress-strain curves of hot tensile tests and was around 5%.
The results obtained in this research show that this behavior of the full size tensile test samples of thin-walled tube (wall thickness less than 0.5 mm) in high temperature (315ºC) is due to the combination of the manufacturing process, the material (crystallographic structure and chemical composition) and the final geometry of the component. In other words, the strong crystallographic texture of material induced by tube drawing process in addition with the geometry of the component are responsible for the behavior in hot uniaxial tensile tests.

## 1. INTRODUCTION

During the life in LWRs (Light Water Reactor) all core materials, including fuel materials and structural components, must satisfy not only standard materials design criteria based on tensile properties, thermal creep, cyclic fatigue and creep-fatigue, but also must provide adequate resistance to two additional overarching environmental degradation phenomena: radiation damage and chemical compatibility (corrosion, stress corrosion cracking, etc.) [1]. Also according to Zinkle et al. [1], although there are many potential areas of concern for materials, the demonstrated highly reliable an operating performance of commercial reactors for the past 10-15 years suggests that most of the problems faced by core components are solved by appropriate materials selection and engineering design. Three specific materials challenges are considered to be of highest importance: (i) exploration of potential further improvements in fuel reliability and operational burn-up limits under normal operating conditions, and safety under transient accident conditions; (ii) corrosion and stress corrosion cracking in reactor components; and (iii) RPV (Reactor Pressure Vessel) integrity,

particularly for life extension scenarios. For example, the shortcomings of the Zr alloy/$UO_2$ fuel system to severe accident conditions such as occurred at the Fukushima Dai-ichi nuclear power plant in Japan following the 2011 earthquake and tsunami has led to increased interest in improving the safety of nuclear reactors to rare but credible accident scenarios [2]. Considering that the key functions of the fuel system in an accident scenario are to maintain core cooling capability and to minimize or prevent dispersion of fuel and fission products, there are at least two major potential approaches to design LWR fuel systems with improved accident tolerance concerning to fuel materials: (i) utilize cladding options by reduced reaction kinetics with high-temperature steam; reduction of the cladding high-temperature oxidation rate by one or more orders of magnitude compared to alloys such as Zircaloy would nearly eliminate the contribution of heat input from oxidation and would proportionally reduce the generation of hydrogen and (ii) utilize fuel cladding with improved high-temperature mechanical properties and resistance to hydrogen embrittlement (high tensile and short-term creep strength, good thermal shock resistance, high melting temperature) [1].

Thus, in this research a possible candidate to be used in the fuel system, a stainless steel type 347, manufactured as seamless thin-walled tubes, was mechanically characterized and because a non usual behavior in hot tensile test, which made impossible the measurement of elongation parameter, it was carefully investigated to understand and explain the phenomena. Many improvements and modifications concerning to tensile test were performed to minimized the interference of misalignment of fixture components and effects of samples assemblies, very critical due to the geometry of the tubes (thin wall).

The studies were concentrated in the material microstructure and crystallographic textures to explain the behavior in uniaxial hot tensile tests.

## 2. MATERIALS AND METHODS

The chemical analysis (ICP-OES - Inductively Coupled Plasma Optical Emission Spectrometry) of the stainless steel tubes used in this study is presented in Table 1.

**Table 1: Chemical analysis of the stainless steel type 347 tubes.**

| Element | C | Mn | P | S | Si | Cr | Ni | Nb+Ta | Fe |
|---|---|---|---|---|---|---|---|---|---|
| Weigth % | 0.041 ± 0.001 | 1.72 ± 0.02 | 0.011 ± 0.001 | 0.003 ± 0.001 | 0.39 ± 0.01 | 17.68 ± 0.19 | 10.95 ± 0.14 | 0.81 ± 0.02 | Bal. |

Fig. 1 shows the microstructure of the material of the tubes in the longitudinal and transversal directions. Electrolytic metallographic attack used was oxalic acid and nitric acid (50%), sequentially. GS (grain size) measurements, obtained in accordance with ASTM E112 standard, indicate ASTM sizes 9.7 and 10 for the longitudinal and transversal directions, respectively, and average hardness, according ASTM E384 standard, was 320 ± 10 HV.

The tensile tests were performed using the design of longitudinal test body "full size", according to the standard ASTM A 370 standard – Annex A2. Specifically, in the tensile tests in high temperature (315ºC), the observed fracture mode presented helical aspect without

separation of tensile sample, which not allowed the measurement of elongation after tests. The other parameters, tensile strength and yield strength, were obtained and found according specified. Tests conducted in solution annealed condition (~1040ºC for 10 minutes) presented normal behavior (complete separation of the sample parts and fracture surfaces in the transversal direction) and all mechanical parameters, including elongation, were correctly measured.

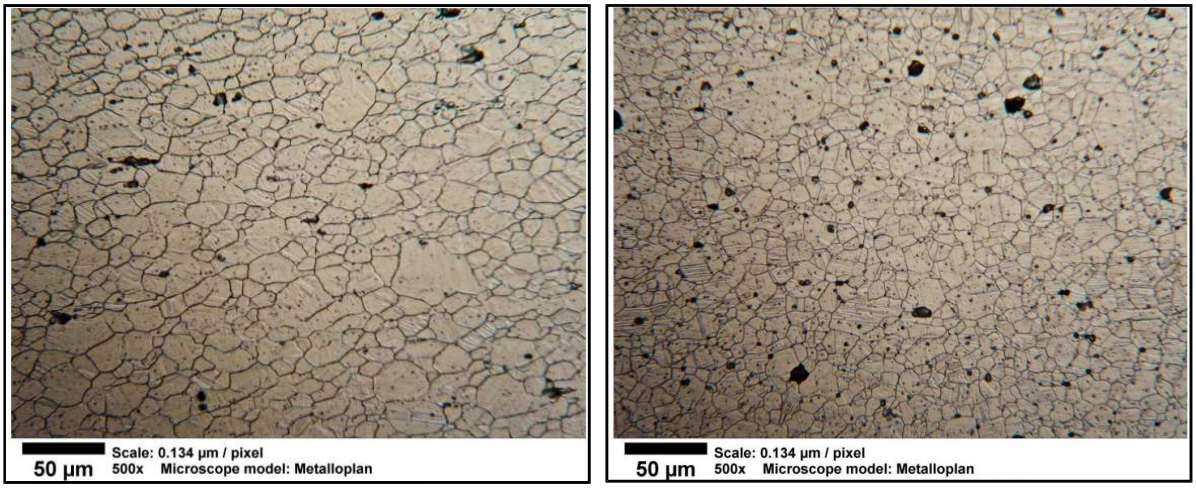


(a) (b)

**Figure 1: Microstructure of stainless steel TP 347 in the longitudinal direction (a), with average GS ASTM 9.7, and in the transversal direction (b), with average GS ASTM 10.**

Stress analysis considering the geometry of the tube, indicated that a small misalignment (1º) in the tensile test sample can produce a stress distribution on the walls of the tube that induce, at one end, stress below the yield strength (YS), while at the other end the stress are already above the tensile strength (TS). Taking this fact into account, several tensile tests were performed in a tensile test machine Instron, model 1331, and the associated furnace (Fig. 2), taking care on the correct alignment of all components.

The X-ray analysis measurements of the tubes material were obtained using a Rigaku X-ray diffractometer, model D-MAX TEXT, with Cr $K_\alpha$ anode, V filter, with scanning range $0 < \alpha < 75^o$ and $0 < b < 360^o$ and the 5º step. The data were processed using the texture analysis program PAT v. 2.6.

## 3. RESULTS AND DISCUSSION

### 3.1. Hot Tensile Tests

Some results of hot tensile tests (315ºC) carried out on the cold-worked tubes are presented in Fig. 3.

The measurements obtained using the stress-strain curves, from the tensile tests, were deducted from the elongation of the sample, considering that was used the full size design of

standard ASTM A 370 standard - Annex A2, where the free section of the tube has the dimension of 50 mm (2 in.).

**Figure 2: Design of the hot tensile test of the tubes, showing the helical mode of fracture.**

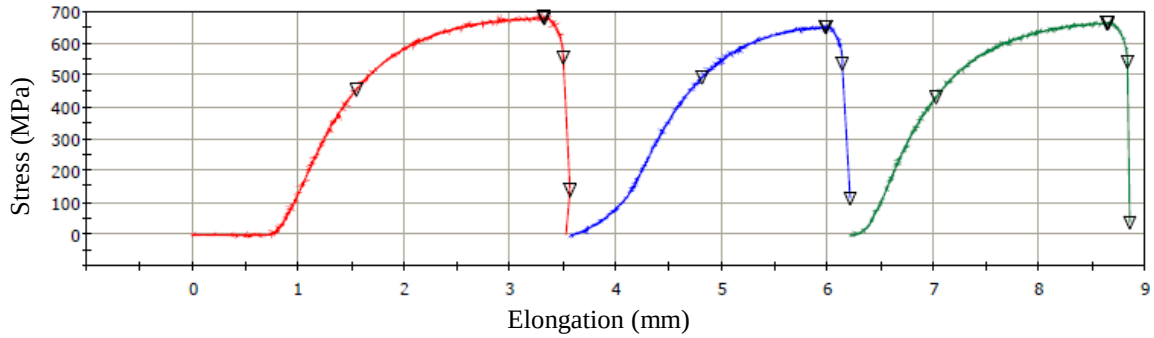


**Figure 3: Results of hot tensile test of stainless steel 347 tubes in cold-worked condition. Average elongation of 5%.**

The microstructural analysis of fracture region (Fig. 4) shows a characteristic mode of ductile fracture, with dimples in the fracture surface. It means, clearly, that the fracture is not fragile or catastrophic, even the very low elongation (average 5%).

The solution annealing heat treatment (~1040ºC for 10 minutes) was performed on cold-worked tubes in order to remove the thermo-mechanical treatment effects on the material due to the manufacturing processing of the tube (drawing). Hot tensile tests were performed to verify if the unconventional fracture behavior was due exclusively to tensile test design and geometry of the tube. The results of the hot tensile test are presented in Fig. 5 and show a significant decrease of mechanical properties, but an average elongation of 42%. The fracture

mode of fracture of all test samples was considered normal, with complete separation of the parts.

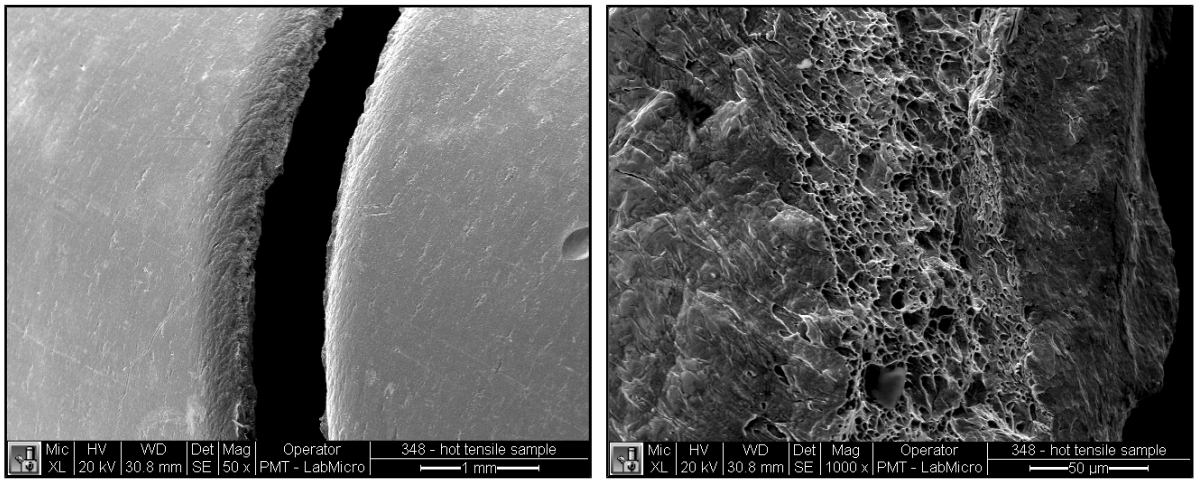


(a) (b)

**Figure 4: SEM image of hot tensile test sample in the fracture region of the tube (a) and detail showing characteristics dimples of ductile fracture.**

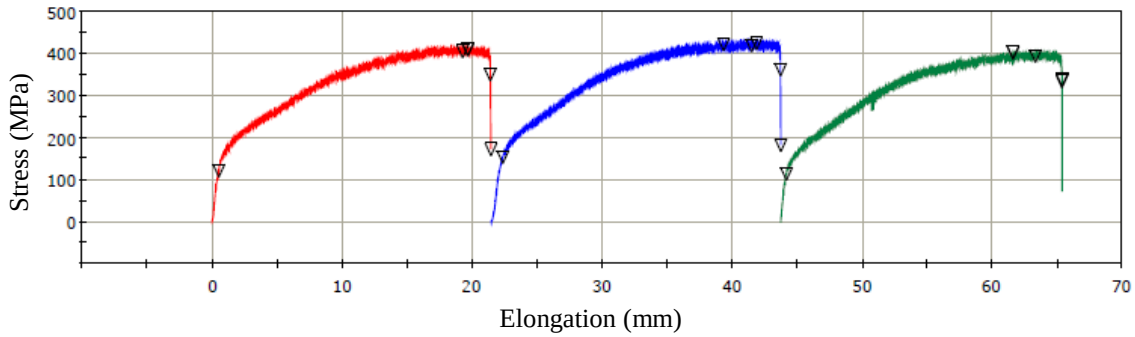


**Figure 5: Results of hot tensile test of solution annealed tubes. Average elongation of 42%.**

### 3.2. Crystallographic Texture Analysis

Austenitic stainless steels have a face-centred cubic (FCC) crystallographic structure, cannot be hardened by heat treatment, but present a substantial increase of mechanical resistance by cold-working. In the solution annealed condition, these steels have a microstructure constituted of insoluble particles or partially insoluble ones, predominantly NbC carbides in case of 347 stainless steel, dispersed in a solid solution that has a low stacking fault energy (SFE) with several annealing twins. During the cold-working of austenitic stainless steels, stacking faults, deformation-induced martensitic phase, deformation twins and deformation bands can be formed, in addition to an intensive dislocation multiplication. The SFE has an important role in the substructure of these steels, *i.e.* in the nature, density and distribution of the lattice defects and the tendency towards martensite formation [3]. In general, a lower SFE makes dislocation cross-slip more difficult, resulting in less dislocation mobility and more

homogeneous dislocation distribution, with less tendency towards the formation of dislocation cells. Also larger amount of stacking faults and deformation-induced martensite (DIM) can be correlated to a lower SFE [4]. The austenitic stainless steels are commonly considered as low SFE materials, but may present, in general, two different microstructures in work-hardened condition: for a high SFE, a cellular dislocation distribution without DIM and, for a low SFE, a planar dislocation distribution containing DIM.

SFEs of more common austenitic stainless steels (Table 2) can be evaluated by means of the Equation 1 suggested by Schramm and Reed [5]:

$$\text{SFE } (mJ/m^2) = -53 + 6.2(\%Ni) + 0.7(\%Cr) + 3.2(\%Mn) + 9.3(\%Mo) \quad (1)$$

**Table 2: Chemical composition (weight %) and SFE ($mJ/m^2$) of some austenitic stainless steels [5].**

| Type | UNS Nº | Werkstoff Nr. | C | Mn | Si | Cr | Ni | Mo | Other | SFE ($mJ/m^2$) |
|---|---|---|---|---|---|---|---|---|---|---|
| 301 | S30100 | 1.4310 | <0.15 | <2.0 | <1.0 | 16.0-18.0 | 6.0-8.0 | --- | --- | <16 |
| 304 | S30400 | 1.4301 | <0.08 | <2.0 | <1.0 | 18.0-20.0 | 8.0-10.5 | --- | --- | 9.2-32.5 |
| 304L | S30403 | 1.4306 | <0.03 | <2.0 | <1.0 | 18.0-20.0 | 8.0-12.0 | --- | --- | 9.2-41.8 |
| 316 | S31600 | 1.4401 | <0.08 | <2.0 | <1.0 | 16.0-18.0 | 10.0-14.0 | 2.0-3.0 | --- | 34.6-80.7 |
| 316L | S31603 | 1.4404 | <0.03 | <2.0 | <1.0 | 16.0-18.0 | 10.0-14.0 | 2.0-3.0 | --- | 34.6-80.7 |
| 321 | S32100 | 1.4541 | <0.08 | <2.0 | <1.0 | 17.0-19.0 | 9.0-12.0 | --- | Ti>5 X%C | 14.7-41.1 |
| 347 | S34700 | 1.4550 | <0.08 | <2.0 | <1.0 | 17.0-19.0 | 9.0-13.0 | --- | Nb>10 X%C | 14.7-47.3 |
| 370(*) | S37000 | 1.4970 | 0.08-0.12 | <2.0 | 0.3-0.55 | 14.5-15.5 | 14.5-15.5 | 1.0-1.4 | Ti= 0.3-0.55 | 56.4-73.4 |
| 370 | S37000 | 1.4970 | 0.08-0.12 | 1.6-2.0 | 0.25 0.45 | 14.5-15.5 | 15.0-16.0 | 1.05 1.4 | Ti= 0.35-0.55 | 65.0-76.5 |

(*) German nuclear specification

The martensite phase formation is, therefore, related to the stress state given by the deformation process. In austenitic stainless steels the temperature below which austenite transforms spontaneously to martensite, *M*s, is less than 0°C. *M*s can be estimated by the Equation 2 of Eichelmann and Hull [6]:

$$M_s\ (°C) = 1305 - [1667(\%C + \%N) + 28(\%Si) + 33(\%Mn) + 42(\%Cr) + 61(\%Ni)] \quad (2)$$

where the contents are in wt%. Since *M*s is low, martensite is not expected to form during the cooling of the austenitic stainless steels. On the other hand, *M*d, temperature below which deformation stresses can initiate the martensitic transformation, is usually above room temperature. The temperature at which 50% of the $\alpha'$ -martensite (CCC structure) is produced after 30% true deformation under tensile condition, can be evaluated with the help of the Equation 3 proposed by Angel [7]:

$$Md_{30/50}\ (°C) = 413 - [462(\%C + \%N) + 9.2(\%Si) + 8.1(\%Mn) + 13.7(\%Cr) + 9.5(\%Ni) + 18.5(\%Mo)] \quad (3)$$

The deformation induced by martensite transformation in the austenitic stainless steels is influenced by the steel chemical composition and by the variables related to the cold-working parameters such as deformation, strain rate, stress state and deformation temperature [3]. In general, the tendency towards martensite formation and martensite quantity increase with equivalent chromium, deformation level, deformation speed and decreases with equivalent nickel, SFE and deformation temperature. Steels that present a higher *M*d temperature, such as the AISI 301 and 304 are highly susceptible to the formation of DIM during deformation at room temperature, whilst steels such as the AISI 316 and 321, with lower *M*d temperatures, the formation of DIM is generally absent at room temperature working [3]. An explanation for such a behavior is that nickel has an accentuated effect in increasing the SFE [4] and in suppressing the formation of DIM [8]. This absence of martensitic phase was also seen in 347 cold-worked tubes, as can be seen in the X-ray diffraction result shown in Fig. 6.

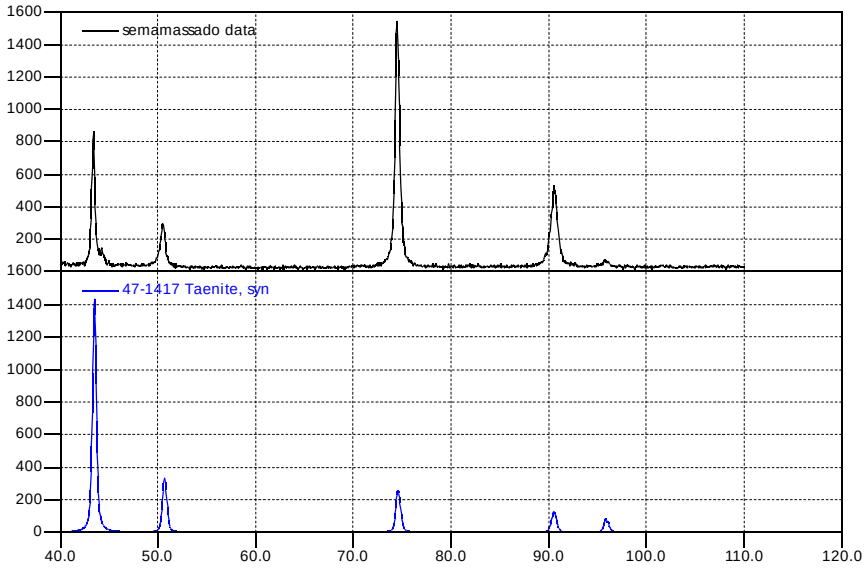


**Figure 6: X-ray diffraction pattern of tube material (347 stainless steel) as received condition. The blue spectrum shows the standard peaks of face-centred cubic structure (typical of austenite).**

The plastic deformation mechanism of austenitic stainless steels (FCC) deals with dislocation slip that appears generally between one of the four close-packed {111} planes and in one of the three <110> directions. More than one slip system can be activated, which is called multi-directional slip. Activation of other slip systems is rarely observed [9,10]. To activate a slip system a critical shear stress acting on a slip plane is required and can be calculated as Equation 4:

$$\tau = \frac{F}{A} \cos\phi.\cos\lambda \tag{4}$$

where $\tau$ is the resolved shear stress from the force $F$ acting on cross section area $A$, $\phi$ is the angle between $F$ and the normal to slip plane and $\lambda$ is the angle between $F$ and the slip direction. The quantity of $\cos\phi.\cos\lambda$ is called the Schmid factor (SF) [9].

Depending on the stresses applied during mechanical processing, directions, intensities and resulting deformation rates, a characteristic texture will be observed in the finished material. For example, cold rolled austenitic stainless steel sheets present a strong crystallographic texture type brass {110} <112> and several other weaker orientation such as {110} <001> (Goss), {135} <211> and {211} <011> [3]. In the drawing process of seamless tube, applied stresses in the material during processing are different from those of a normal process of rolling and the texture observed in 347 stainless steel presented a strong crystallographic texture type Goss {110} <001>, as shown in Fig. 7.

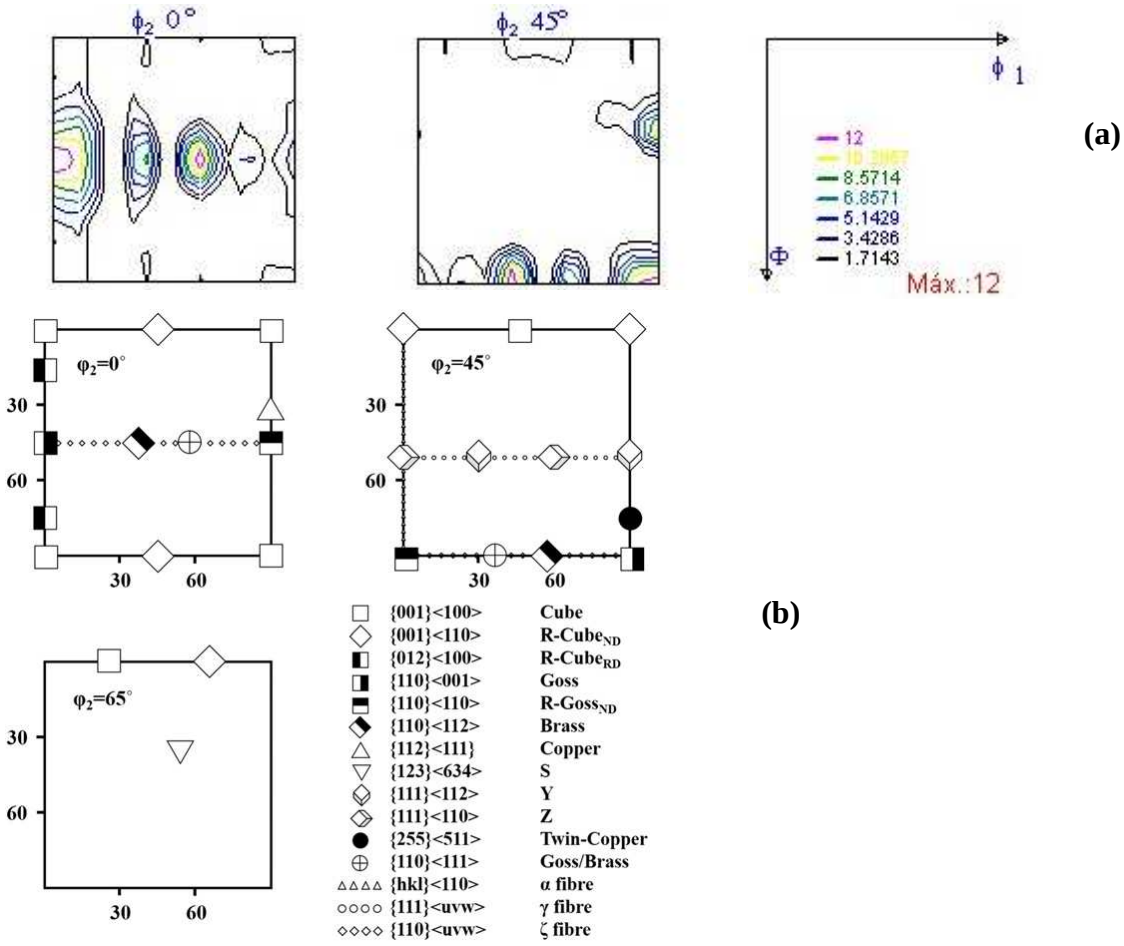


**Figure 7: (a) Orientation distribution functions (ODF) in sections $\varphi_2$ = 0º and 45º for austenite for 347 stainless steel tube material in as received condition and (b) main orientations and fibers observed in steels. It was observed that the 347 stainless steel tube present strong texture type Goss {110}<001>, with TR (*times random*) of 11.8; type Brass {110} <112>, with TR of 8.0; and type Goss/Brass {110}<111>, with TR of 12.**

The active slip systems observed in austenitic stainless steels (FCC) are {111} <110> with higher values of SF. On a microscopic level, the material grains deformation is dependent on the SF which affects the shear stress in a given slip system. Greater SF on a slip system increases the probability of activating the dislocations movement in the system due to the increased resultant shear stress, generating plastic deformation. This phenomenon is also dependent on the SF of the neighbors grains and which slip systems are active in these grains.

Noting the texture obtained in 347 stainless steel of drawn tube, it can be seen that the angle between the planes {110} and plans of slipping {111} is approximately 35.3° [11] and the other textures do not induce slipping in {111} <110> systems.

In terms of recrystallization, the smaller the SFE, considering constant all other process variables, the greater stored energy during deformation and corresponding activation energy for the process of recrystallization. The nucleation of recrystallization begins on deformation bands of and the vicinity of grain boundaries [12]. In general, recrystallization of austenitic stainless steels and recrystallization temperature in particular depend on several factors such as the steel type, the heat treatments that steel might have been submitted before cold-working, the quantity, mode, temperature and strain rate at cold-working, as well as the heating rate and holding time at annealing temperature. In general, all variables that increase the stored energy due to deformation, such as a decrease of SFE, increase in strain, increased strain rate and decrease in deformation temperature, cause a decrease in the recrystallization temperature.

Also, secondary precipitates, as NbC type in 347 stainless steel, in the same temperature range and times in which recrystallization occurs and both phenomena present a strong interaction: cold-working accelerates precipitation and precipitation delays recrystallization. The effect mostly found and expected is that the precipitation of MC in the dislocation substructure, introduced by cold-working, hinders dislocation rearrangement and delays recrystallization by grain boundary pinning [13,14].

Several studies have shown that the texture of solution annealed materials obtained by different cold-working processes is related to previous deformation texture [3]. This fact shows that, depending on the degree and rate of deformation imposed on the material, the orientation of the recrystallized grains after recrystallization process is not random, but rather directed [15].

Crystallographic texture analysis of 347 stainless steel tube after solution annealing heat treatment at ~1040º C for 10 minutes, also show no change in the texture when compared to the tube in as received condition (Fig. 8).

This demonstrates that during manufacturing process of 347 stainless steel tube, involving four drawing steps interspersed with high annealing heat treatments (~1040ºC), do not result in a microstructure with randomly oriented grains; on the contrary, the strong crystallographic texture of drawn tube is maintained after solution annealing heat treatments.

The macroscopic differences from the non-linear region of stress-strain curves between room temperature and high temperature (315ºC) can be explained by different behavior on a microscopic level. Several studies have shown a greater level of average grain misorientation

(GAM) at room temperature than at high temperatures for similar degrees of deformation [16]. In plastically deformed materials, the local misorientation is related to plastic deformation and an average value of misorientation is measured between all points in the grain. At high temperatures, the dislocation movements can be faster than at room temperature due to thermal activation, but it is also affected by other processes controlled by diffusion as the dynamic strain aging (DSA). The DSA originates from the interaction between solute atoms and dislocations during plastic deformation. Under plastic flow, dislocations are gliding until they come across an obstacle where they are stationary until the obstacles are surmounted. When the dislocations are stationary, solute atoms can diffuse towards the dislocations which result in an increase in the activation energy for re-activation and consequently also an increase in the stress needed for overcoming the obstacle [17-19]. Thus, DSA is directly influenced by the deformation rate that affects the mobility of the dislocations and the temperature that influences the diffusion rate of solute atoms. The temperature regime of DSA is from 200 to 800°C for austenitic materials (FCC) and for austenitic stainless steels at temperatures below 350ºC carbon is responsible for DSA while nitrogen and/or substitutional chromium atoms are responsible at higher temperatures (400 to 650ºC) [20]. DSA is characterized by serrated yielding occurring in the stress-strain curve, denoted as Portevin-Le Châtelier (PLC) effect or jerky flow (Fig. 5), created by the pinning and unpinning of dislocations [21-23]. The expected deformation in the DSA regime is planar slip and slip bands in single and multi-direction [24]. Local damage has been connected to interaction between slip bands and/or interaction between twins and grain boundaries.

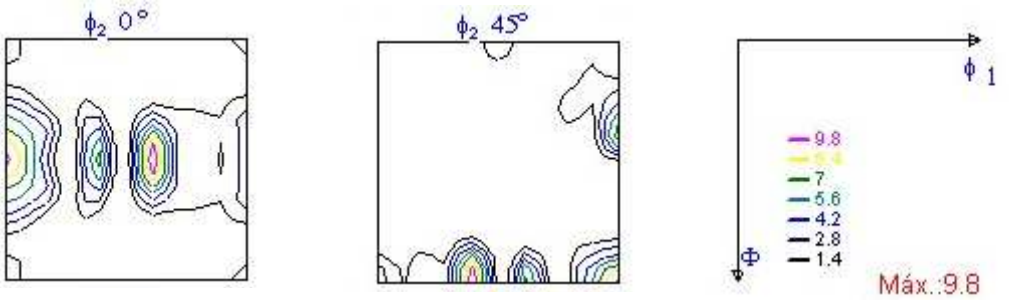


**Figure 8: Orientation distribution functions (ODF) in sections $\varphi_2$ = 0º and 45º for austenite for 347 stainless steel tube material after solution annealing heat treatment at ~1040ºC for 10 minutes. It was observed that the solution annealed 347 stainless steel tube preserved drawn tube texture type Goss {110}<001>, with TR (*times random*) of 9.0; type Brass {110} <112>, with TR of 6.6; and type Goss/Brass {110}<111>, with TR of 9.8.**

Considering the crystallographic texture of 347 stainless steel tube (cold-worked), where the slipping systems (FCC structure) are {111} <110> and the angle with the {110} of Goss texture being around 35º, it is expected that in an uniaxial tension test the fracture cracks shall be nucleated in these slip systems. Measurements of the angles of cracks observed in the tensile tests of 347 stainless steel tube at 315ºC show angles close to 35º (Fig. 9), which confirms the indication of cracks nucleation in these directions due to the crystallographic texture observed in these tubes.

Specifically a research developed by some researchers [16], using a Sandvik tube, investigate the microstructure of austenitic steel by electron back-scattered diffraction technique (EBSD) with in-situ tensile test on a SEM. It was analyzed the behavior at RT and 300ºC, obtaining

12.35% and 4.85% elongation in the two temperatures, respectively. The metallurgical conditions of the tube were not mentioned, but the tensile samples were removed from longitudinal (axial) direction of the tube and the results showed that the active slip system was the {111} <110> and the cracks were observed (nucleation and propagation) along slip systems with higher SF values.

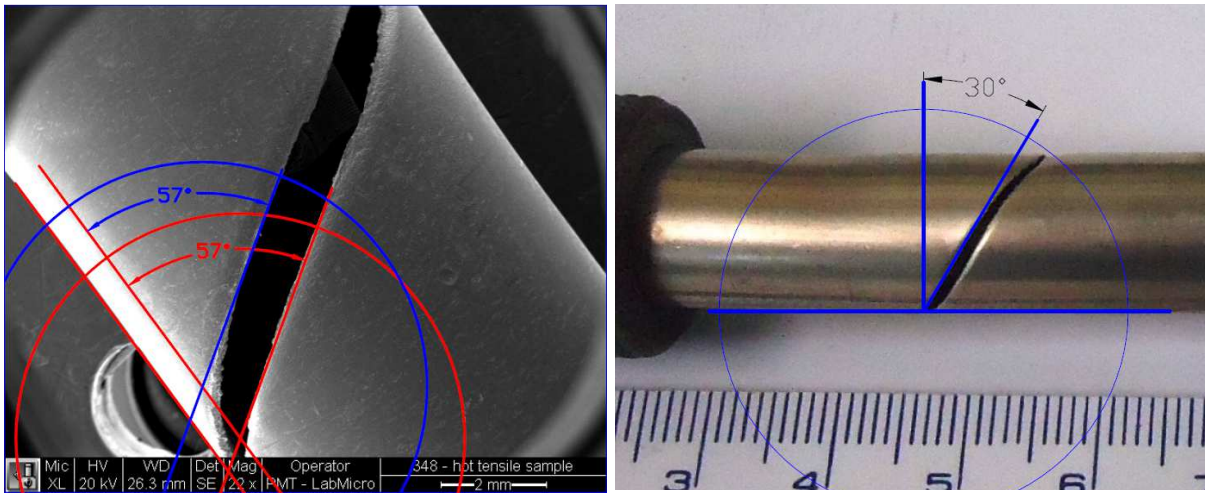


**(a)** **(b)**

**Figure 9: (a) SEM image of the cold-worked 347 stainless steel tube after hot tensile test showing the measurement of the angle of crack in the middle region of fracture with the longitudinal direction of the tube, and the angle of 33º is measured perpendicular to the rolling direction and (b) macroscopic image of other hot tensile tube sample with the measurement of the angle of crack direction perpendicular to the rolling direction.**

Several researches with metals and alloys with different crystallographic structures show that textures induced by mechanical processes [25-27], such as rolling, can be modified through high degrees of cold-working, when the density of defects in the structure of the material is high enough to promote more isotropic recrystallization (grain nucleation with random crystallographic orientation) during annealing. In commercial thin-walled seamless tubes obtained by drawing process these high degrees of plastic deformation hardly are applied, since it incurs in application of better and more resistant tools, as well as in risks of rupture of the component due to the lower break resistant section.

## 3. CONCLUSIONS

The results obtained in this research show that the unconventional mode of rupture of the full size tensile test samples of thin-walled stainless steel tube type 347 in high temperature (315ºC) is due to the combination of the manufacturing process, the material (crystallographic structure and chemical composition) and the final geometry of the component (thin-walled tube). In other words, the strong crystallographic texture of material induced by tube drawing process in addition with the geometry of the component are responsible for the behavior in hot uniaxial tensile tests. Specifically in these tests, the tensile test sample design is also quite susceptible to minimum misalignments between the sample

and fixation fasteners of the tensile test machine. However, even with the complete separation after hot tensile test observed in very few samples, the fracture was observed in inclined direction, instead of the expected direction (transversal).

An alternative manufacturing process condition in order to minimize the effect of crystallographic texture of the seamless drawing tubes would be an application of high degrees of cold-working, when the density of defects in the structure of the material is high enough to promote more isotropic recrystallization (grain nucleation with random crystallographic orientation) during annealing, but it incurs in the use of better and more resistant tools, as well as in risks of rupture of the component due to the lower break resistant section.

These tubes, in the metallurgical condition reach satisfactory mechanical properties at high temperature (315ºC) as the tensile strength and yield strength, and the average value of elongation obtained from stress-strain curves of hot tensile tests was 5%. The fracture mode was ductile despite the lower elongation values.

## ACKNOWLEDGMENTS

The authors would like to thank CTMSP (Brazilian Navy Technological Center), for material supply and permission to perform the tests and analysis, and IPEN/CNEN-SP (Energy and Nuclear Research Institute), for the X-ray diffraction and crystallographic texture analysis performed in the Materials Science and Technology Center (CCTM/IPEN).

## REFERENCES

1. S. J. Zinkle, G. S. Was, “Materials Challenges in Nuclear Energy,” *Acta Mater.,* **61,** pp.735-758 (2013).
2. The ASME Presidential Task Force on Response to Japan Nuclear Power Plant Events, *Forging a New Nuclear Safety Construct*, New York: American Society of Mechanical Engineers (2012).
3. A. F. Padilha, R. L. Plaut, P. R. Rios, “Annealing of Cold-Worked Austenitic Stainless Steels,” *ISIJ International*, **43(2)**, pp.135-143 (2003).
4. R. P. Reed, *Austenitic Steels at Low Temperatures*, Ed. by R. P. Reed and T. Horiuchi, Plenum Press, N.Y., p.41 (1983).
5. R. E. Schramm, R. P. Reed, “Stacking Fault Energies of Seven Commercial Austenitic Stainless Steels,” *Metall. Trans.*, **6A**, pp.1345 (1975).
6. G. H. Eichelmann, F. C. Hull, “The Effect of Composition of Spontaneous Transformation of Austenite to Martensite in 18-8-Type Stainless Steel,” *Trans. Am. Soc. Met.*, **45**, pp.77 (1953).
7. T. Angel, “Formation of Martensite in Austenitic Stainless Steels,” *J. Iron Steel Inst.*, **177**, pp.165 (1954).
8. A. Weib, X. Fang, H.- J A. Eckstein, “Effect of Cryoforming of Austenitic Cr Ni-Steels at 77 K on Martensitic-Transformation and Work-Hardening Characteristics,” *Steel Res.*, **66(11)**, pp.495 (1995).
9. D. Hull, D. J. Bacon, *Introduction to Dislocations*, Butterworth-Heinmann (2007).

10. R. W. Hertzberg, *Deformation and Fracture Mechanics of Engineering Materials*, John Wiley & Sons (1995).
11. 15. B. D. Cullity, *Elements of X Ray Diffraction,* Addison-Wesley Publishing Company, Inc. (1956).
12. L. F. M. Martins, R. L. Plaut, A. F. Padilha, "Effect of Carbon on the Cold-Worked State and Annealing Behavior of 21wt%Cr-8wt%Ni Austenitic Stainless Steels," *ISIJ International*, **38(6)**, pp.572 (1998).
13. E. J. Herrera, V. Ramaswamy, D. R. F. West, *J. Iron Steel Inst.*, **211**, pp.229 (1973).
14. M. Vasudevan, S. Venkadesan, P. V. ivaprasad, "Influence of Ti/(C+6/7N) Ratio on the Recrystallization Behaviour of a Cold Worked 15Cr-15Ni-2.2Mo-Ti Modified Austenitic Stainless Steel," *J. Nucl. Mater.*, **231**, pp.231 (1996).
15. M. J. Dickson, D. Green, "The Cold-Rolling and Primary-Recrystallisation Textures of 18% Chromium Steels Containing 10%, 12% and 14 % Nickel," *Mater. Sci. Eng.*, **4**, pp.304 (1969).
16. M. Calmunger, R. Peng, G. Chai, S. Johansson, J. Moverare, "Advanced microstructure studies of an austenitic material using EBSD in elevated temperature in-situ tensile testing in SEM," *Key Eng. Mater.*, pp.497 (2014).
17. L. H. Almeida, I. Le May, P. R. O. Emygdio, "Mechanistic Modeling of Dynamic Strain Aging in Austenitic Stainless Steels," *Mater. Charact.*, **41**, pp.137 (1998).
18. A. Van Den Beukel, "On the Mechanism of Serrated Yielding and Dynamic Strain Ageing," *Acta Metal.*, **28**, pp.965 (1980).
19. R. A. Mulford, U. F. Kocks, "New observations on the mechanisms of dynamic strain aging and of jerky flow," *Acta Metal.*, **27**, pp.1125 (1979).
20. G. V. P. Reddy, R. Sandhya, K. B. S Rao, S. Sankaran, "Influence of Nitrogen Alloying on Dynamic Strain Ageing Regimes in Low Cycle Fatigue of AISI 316LN Stainless Steel," *Procedia Eng.*, **2**, pp.2181–2188 (2010).
21. I. Nikulin, R. Kaibyshev, "Deformation Behavior and the Portevin-Le Chatelier Effect in a Modified 18Cr-8N Stainless Steel," *Mater. Sci. Eng. A*, **528**, pp.1340 (2011).
22. W. Karlsen, M. Ivanchenko, U. Ehrnstén, Y. Yagodzinskyy, H. Hänninen, "Microstructural manifestation of dynamic strain aging in AISI 316 stainless steel," *J. Nucl. Mat.*, **395**, pp.156 (2009).
23. M. C. Cai, L. S. Niu, T. Yu, H. J. Shi, X. F. Ma, "Strain Rate and Temperature Effects on the Critical Strain for Portevin-Le Châtelier Effect," *Mater. Sci. Eng. A*, **527**, pp.5175 (2010).
24. M. Calmunger, "High Temperature Behavior of Austenitic Alloys – Influence of Temperature and Strain Rate on Mechanical Properties and Microstructural Development," *Linköping Studies in Science and Technology*, Thesis No. 1619 (2013).
25. R. K. Roy, "Recrystallization Behavior of Commercial Purity Aluminium Alloys," *Light Metal Alloys Applications*, Dr. Waldemar A. Monteiro (Ed.), In Tech, DOI: 10.5772/58385 (2014).
26. K. Kashihara, H. Inagaki, "Effect of Precipitation on Development of Recrystallization Texture in a 6061 Aluminum Alloy," *Mater. Trans.*, **50**, No. 3, pp.528 (2009).
27. E. Ahmad; F. Karim, K. Saeed, T. Manzoor, G. H. Zahid, "Effect of Cold Rolling and Annealing on the Grain Refinement of Low Alloy Steel," *IOP Conf. Series: Mater. Sci. Eng.*, **60** (2014).